A HYBRID AGGRESSIVE SPACE MAPPING ALGORITHM FOR EM OPTIMIZATION

M.H. Bakr, J.W. Bandler, N. Georgieva and K. Madsen

SOS-99-9-R

March 1999

A HYBRID AGGRESSIVE SPACE MAPPING ALGORITHM FOR EM OPTIMIZATION

Mohamed H. Bakr, *Student Member, IEEE*, John W. Bandler, *Fellow, IEEE*, Natalia Georgieva, *Member, IEEE*, and Kaj Madsen

Abstract We propose a novel Hybrid Aggressive Space Mapping (HASM) optimization algorithm. HASM exploits both the Trust Region Aggressive Space Mapping (TRASM) strategy and direct optimization. Severe differences between the coarse and fine models and nonuniqueness of the parameter extraction procedure may cause the TRASM algorithm to be trapped in local minima. The HASM algorithm is based on a novel lemma that enables smooth switching from the TRASM optimization to direct optimization if the TRASM algorithm is not converging. It also enables switching back from direct optimization to the TRASM algorithm in a smooth way. The uniqueness of the extraction step is improved by utilizing a good starting point. The algorithm does not assume that the final space-mapped design is the true optimal design and is robust against severe misalignment between the coarse and fine models. The new algorithm has been tested on designs of several microwave filters and transformers. The examples include a three-section and a seven-section waveguide transformer as well as the design of an H-plane waveguide filter and a double-folded stub filter.

This work was supported in part by the Natural Sciences and Engineering Research Council of Canada under Grants OGP0007239, STP0201832 and through the Micronet Network of Centres of Excellence. N. Georgieva is supported by an NSERC Postdoctorate Fellowship and M.H. Bakr by an Ontario Graduate Scholarship.

M.H. Bakr, J.W. Bandler and N. Georgieva are with the Simulation Optimization Systems Research Laboratory and the Department of Electrical and Computer Engineering, McMaster University, Hamilton, Ontario, Canada, L8S 4K1.

J.W. Bandler is also with Bandler Corporation, P.O. Box 8083, Dundas, Ontario, Canada L9H 5E7.

K. Madsen is with the Department of Mathematical Modelling, Technical University of Denmark, DK-2800 Lyngby, Denmark.

I. INTRODUCTION

In this work a Hybrid Aggressive Space Mapping (HASM) algorithm is presented. Space Mapping (SM) optimization [1-4] assumes that the circuit under consideration can be simulated using two models: a fine model and a coarse model. The fine model is accurate but is computationally intensive, e.g., a full-wave EM simulator. The coarse model is assumed to be fast but not very accurate. SM optimization directs most of the optimization computational effort towards the coarse model while maintaining the accuracy of the fine model. The overall computational effort needed is much smaller than that for direct optimization.

Parameter extraction is crucial to the Aggressive Space Mapping (ASM) technique [4]. Here, a coarse model point whose response matches a given fine model response is obtained. This is essentially an optimization problem. The nonuniqueness of the extracted parameters may lead to divergence or oscillation of the iterations [2]. To alleviate this problem the TRASM algorithm was introduced [3]. TRASM integrates a trust region methodology [5] with the ASM technique. Also, it utilizes a recursive multi-point parameter extraction in order to improve the uniqueness of the extraction step.

In this work we address the convergence behavior of the TRASM algorithm. We discuss the effect of a severely misaligned coarse model. We show that in this case TRASM optimization may be trapped in local minima.

The design obtained by pure SM optimization in most cases is very near optimal. However, the optimality of the final design can not be guaranteed. This is because the final space-mapped response matches the optimal coarse model response, which may be different from the optimal fine model response obtained by solving the original design problem in the fine model space.

Our HASM algorithm is designed to overcome these limitations. The algorithm switches smoothly between SM optimization and direct optimization and vice versa. A novel lemma enables such a switch. The algorithm also integrates a novel prediction of the starting point for the parameter extraction problem to enhance the uniqueness.

We start by giving a brief review of SM algorithms in Section II. Some properties of SM optimization that justify utilizing a hybrid algorithm are discussed in Section III. The novel lemma and the prediction approach are introduced in Sections IV and V, respectively. The HASM algorithm is presented in Section VI. The algorithm is applied successfully to the design of microwave transformers and filters. The examples include the design of a three-section waveguide transformer, a seven-section waveguide transformer, an H-plane waveguide filter and a double-folded stub microstrip filter. These examples are given in Section VII. Finally, the conclusions are given in Section VIII.

II. SPACE MAPPING: A BRIEF REVIEW

We refer to the vectors of "fine" model parameters and "coarse" model parameters as $\boldsymbol{x}_{em}$ and $\boldsymbol{x}_{os}$, respectively. The first step in any SM algorithm is to obtain the optimal design of the coarse model $\boldsymbol{x}_{os}^{*}$. The corresponding response is denoted by $\boldsymbol{R}_{os}^{*}$. ASM aims at establishing a mapping $\boldsymbol{P}$ between the two spaces [4]

$$\boldsymbol{x}_{os} = \boldsymbol{P}(\boldsymbol{x}_{em}) \tag{1}$$

such that

$$\left\| \boldsymbol{R}_{em}(\boldsymbol{x}_{em}) - \boldsymbol{R}_{os}(\boldsymbol{x}_{os}) \right\| \le e \tag{2}$$

where $\boldsymbol{R}_{em}$ is the vector of fine model response, $\boldsymbol{R}_{os}$ is the vector of coarse mode response and $\| \ \|$ is a suitable norm. We define the error function

$$\boldsymbol{f} = \boldsymbol{P}(\boldsymbol{x}_{em}) - \boldsymbol{x}_{os}^{*} \tag{3}$$

The final fine model design is obtained and the mapping is established by solving the nonlinear system

$$\boldsymbol{f}(\boldsymbol{x}_{em}) = \boldsymbol{0} \tag{4}$$

Let $\boldsymbol{x}_{em}^{(i)}$ be the ith iterate in the solution of (4). In the ASM technique, the next iterate $\boldsymbol{x}_{em}^{(i+1)}$ is found by a quasi-Newton iteration

$$\boldsymbol{x}_{em}^{(i+1)} = \boldsymbol{x}_{em}^{(i)} + \boldsymbol{h}^{(i)} \tag{5}$$

where $\boldsymbol{h}^{(i)}$ is obtained from

$$\boldsymbol{B}^{(i)}\boldsymbol{h}^{(i)} = -\boldsymbol{f}(\boldsymbol{x}_{em}^{(i)}) \tag{6}$$

and $\boldsymbol{B}^{(i)}$ is an approximation to the Jacobian of the vector $\boldsymbol{f}$ with respect to $\boldsymbol{x}_{em}$ at the *i*th iteration. The matrix $\boldsymbol{B}$ is updated at each iteration using Broyden's update [6].

Vector $\boldsymbol{f}$ is obtained by evaluating $\boldsymbol{P}(\boldsymbol{x}_{em})$, which is done indirectly through parameter extraction. The nonuniqueness of this problem may lead to divergence or oscillation of the ASM technique. The TRASM algorithm [3] was designed to overcome this problem. At the *i*th iteration, the residual vector $\boldsymbol{f}^{(i)} = \boldsymbol{P}(\boldsymbol{x}_{em}^{(i)}) - \boldsymbol{x}_{os}^{*}$ defines the difference between the vector of extracted coarse model parameters $\boldsymbol{x}_{os}^{(i)} = \boldsymbol{P}(\boldsymbol{x}_{em}^{(i)})$ and the optimal coarse model design. The value $\left\| \boldsymbol{f}^{(i)} \right\|$ serves as a measure of the misalignment between the two spaces in the *i*th iteration. The TRASM algorithm aims at minimizing $\left\| \boldsymbol{f}^{(i)} \right\|$. The *i*th iteration of the algorithm is given by

$$(\boldsymbol{B}^{(i)T}\boldsymbol{B}^{(i)} + l\,\boldsymbol{I})\,\boldsymbol{h}^{(i)} = -\boldsymbol{B}^{(i)T}\boldsymbol{f}^{(i)} \tag{7}$$

Parameter l is selected such that the step obtained satisfies $\left\| \boldsymbol{h}^{(i)} \right\| \le d$, where d is the size of the trust region.

III. SOME PROPERTIES OF SPACE MAPPING

ASM and TRASM are efficient algorithms. The number of fine model simulations needed to obtain the space-mapped design is of the order of the problem dimensionality. However, both algorithms depend on the existence of a coarse model that is fast and has enough accuracy.

If the coarse model is bad (i.e., very different from the fine model) space mapping might not work. To illustrate this we consider the Rosenbrock function [7]. We form an artificial problem in which the "coarse" model is given by

$$R_{os} = 100\,(x_2 - x_1^2)^2 + (1 - x_1)^2 \tag{8}$$

and the "fine" model by

$$R_{em} = 100\,((x_2+\alpha_2)-(x_1+\alpha_1)^2)^2 + (1-(x_1+\alpha_1))^2 \tag{9}$$

where a_1 and a_2 are constant shifts. The target of the direct optimization problem is to minimize R_{em}. Considering (8) and (9) we notice that $\boldsymbol{x}_{os}^* = [1.0 \quad 1.0]^T$ and $\boldsymbol{x}_{em}^* = (\boldsymbol{x}_{os}^* - a)$ where $a = [a_1 \quad a_2]^T$. The misalignment between the two models is thus given by the two shifts a_1 and a_2.

We discuss two sets of values for the shifts. First, we consider $a = [-0.1 \quad -0.1]^T$. Using (8) and (9) we notice that the coarse model point whose response matches the fine response at a point $\boldsymbol{x}_{em}$ is $\boldsymbol{x}_{os} = (\boldsymbol{x}_{em} + a)$. It follows that the mapping between the two spaces is given by $\boldsymbol{P}(\boldsymbol{x}_{em}) = \boldsymbol{x}_{em} + a$. The contours of $\left\|\boldsymbol{x}_{em}+a-\boldsymbol{x}_{os}^*\right\|_2^2$ are shown in Fig. 1(a). The mapping $\boldsymbol{P}(\boldsymbol{x}_{em})$ is then approximated through multi-point parameter extraction [3]. Only one perturbed fine model point is utilized. The contours of $\left\|\boldsymbol{P}(\boldsymbol{x}_{em})-\boldsymbol{x}_{os}^*\right\|_2^2$ obtained in this manner are shown in Fig. 1(b). Figs. 1(a) and 1(b) show that $\|\boldsymbol{f}\|_2^2$ has a single minimum which is the solution that would have been obtained by direct optimization. The differences between the two plots are attributed to the nonuniqueness of the parameter extraction process. Taking the point $\boldsymbol{x}_{os}^*$ as the initial solution of the fine model, the TRASM algorithm is expected to converge to $\boldsymbol{x}_{em}^*$. The corresponding contours of R_{em} are shown in Fig. 1(c), whose minimum value is at $[1.1 \quad 1.1]^T$ as expected.

The same steps are repeated for the case $a = [-1.5 \quad -1.5]^T$. The contour plot of $\left\|\boldsymbol{x}_{em}+a-\boldsymbol{x}_{os}^*\right\|_2^2$ is shown in Fig. 2(a). The contour plot of $\left\|\boldsymbol{P}(\boldsymbol{x}_{em})-\boldsymbol{x}_{os}^*\right\|_2^2$ obtained using parameter extraction is shown in Fig. 2(b). Fig. 2(b) illustrates the existence of a minimum of $\left\|\boldsymbol{P}(\boldsymbol{x}_{em})-\boldsymbol{x}_{os}^*\right\|_2^2$ other than $\boldsymbol{x}_{em}^*$ which is closer to the starting point of the TRASM algorithm $\boldsymbol{x}_{os}^*$. It follows that the TRASM algorithm is unlikely to converge to $\boldsymbol{x}_{em}^*$. The corresponding contours of R_{em} for this case are shown in Fig. 2(c), whose minimum value is at $[2.5 \quad 2.5]^T$.

The solution obtained using SM optimization is very near optimal if $\boldsymbol{R}_{os}^{*}$ is similar to the optimal fine model response $\boldsymbol{R}_{em}^{*}$. However, this can not be guaranteed. For example, consider

$$R_{em} = 100\,(x_2 - x_1^2)^2 + (1 - x_1)^2 \tag{10}$$

Assume also that

$$R_{os} = R_{em} + e \tag{11}$$

where $e > 0$. It is clear that R_{os}^{*} is equal to e while R_{em}^{*} is zero. It follows that space mapping may converge to a solution other than $\boldsymbol{x}_{em}^{*}$.

IV. SPACE MAPPING AND DIRECT OPTIMIZATION

The properties of space mapping suggest that a hybrid algorithm be used. This algorithm exploits the efficiency of space mapping and defaults to direct optimization when space mapping fails. Our HASM algorithm utilizes a novel lemma that enables smooth switching between the TRASM algorithm and direct optimization and vice versa.

Lemma Assume that $\boldsymbol{x}_{os}$ corresponds to $\boldsymbol{x}_{em}$ through a parameter extraction process. Then the Jacobian $\boldsymbol{J}_{em}$ of the fine model response at $\boldsymbol{x}_{em}$ and the Jacobian $\boldsymbol{J}_{os}$ of the coarse model response at $\boldsymbol{x}_{os}$ are related by

$$\boldsymbol{J}_{em} = \boldsymbol{J}_{os}\,\boldsymbol{B} \tag{12}$$

where $\boldsymbol{B}$ is a valid mapping between the two spaces at $\boldsymbol{x}_{os}$ and $\boldsymbol{x}_{em}$.

Proof

As the points $\boldsymbol{x}_{em}$ and $\boldsymbol{x}_{os}$ correspond to each other, it follows that their responses match, i.e.,

$$\boldsymbol{R}_{em}(\boldsymbol{x}_{em}) = \boldsymbol{R}_{os}(\boldsymbol{x}_{os}) \tag{13}$$

Now define a new fine model point $\boldsymbol{x}_n = \boldsymbol{x}_{em} + \Delta\,\boldsymbol{x}_{em}$ where $\Delta\boldsymbol{x}_{em}$ is a small perturbation. The response at this new point is perturbed from the response at the point $\boldsymbol{x}_{em}$ by

$$\Delta \boldsymbol{R} = \boldsymbol{J}_{em} \Delta \boldsymbol{x}_{em} \tag{14}$$

The point $\boldsymbol{x}_n$ corresponds to a coarse model point $\boldsymbol{x}_{os} + \Delta \boldsymbol{x}_{os}$ that satisfies

$$\Delta \boldsymbol{R} = \boldsymbol{J}_{em} \Delta \boldsymbol{x}_{em} = \boldsymbol{J}_{os} \Delta \boldsymbol{x}_{os} \tag{15}$$

Also, by definition of the mapping $\boldsymbol{B}$ the two perturbations $\Delta \boldsymbol{x}_{em}$ and $\Delta \boldsymbol{x}_{os}$ are related by

$$\boldsymbol{B} \Delta \boldsymbol{x}_{em} = \Delta \boldsymbol{x}_{os} \tag{16}$$

multiplying both sides of (16) by $\boldsymbol{J}_{os}$ we get

$$\boldsymbol{J}_{os} \boldsymbol{B} \Delta \boldsymbol{x}_{em} = \boldsymbol{J}_{os} \Delta \boldsymbol{x}_{os} \tag{17}$$

Comparing (17) with (15) we conclude that

$$\boldsymbol{J}_{em} = \boldsymbol{J}_{os} \boldsymbol{B} \tag{18}$$

Relation (18) is interesting. It shows that by having the matrix $\boldsymbol{B}$ and the coarse model Jacobian $\boldsymbol{J}_{os}$ we are able to obtain a good estimate of the Jacobian of the fine model response without any further fine model simulations. It follows that when SM optimization is not converging smoothly we can switch to direct optimization and supply it with the available first order derivatives given by (18).

Another relationship which can be easily obtained from (18) is

$$\boldsymbol{B} = \left(\boldsymbol{J}_{os}^T \boldsymbol{J}_{os} \right)^{-1} \boldsymbol{J}_{os}^T \boldsymbol{J}_{em} \tag{19}$$

Relation (19) assumes that $\boldsymbol{J}_{os}$ is full rank and $m \geq n$, where n is the number of parameters and m is the dimensionality of both $\boldsymbol{R}_{em}$ and $\boldsymbol{R}_{os}$. It is used for switching back from direct optimization to SM optimization. Fig. 3 illustrates the switching between SM optimization and direct optimization.

We illustrate the lemma as follows. Consider

$$R_{em} = (0.9x_1 + 0.1x_2)^2 + (0.1x_1 + 0.9x_2)^2 \tag{20}$$

and

$$R_{os} = x_1^2 + x_2^2 \tag{21}$$

Take $\boldsymbol{x}_{em} = [2.0 \quad 1.0]^T$. Here R_{em} = 4.82. The solution for the parameter extraction problem is $\boldsymbol{x}_{os} = [1.90 \quad 1.10]^T$. The Jacobian $\boldsymbol{J}_{os}$ at $\boldsymbol{x}_{os}$ is

$$\boldsymbol{J}_{OS} = \begin{bmatrix} 3.8 & 2.2 \end{bmatrix} \tag{22}$$

From (20) and (21) it is seen that

$$\boldsymbol{B} = \begin{bmatrix} 0.9 & 0.1 \\ 0.1 & 0.9 \end{bmatrix} \tag{23}$$

It follows that $\boldsymbol{J}_{em}$ at $\boldsymbol{x}_{em}$ is estimated by

$$\boldsymbol{J}_{em} = \begin{bmatrix} 3.8 & 2.2 \end{bmatrix} \begin{bmatrix} 0.9 & 0.1 \\ 0.1 & 0.9 \end{bmatrix} = \begin{bmatrix} 3.64 & 2.36 \end{bmatrix} \tag{24}$$

which is the exact Jacobian of the fine model response.

V. SELECTION OF THE STARTING POINT

The discussion in Section III reveals how the nonuniqueness of the parameter extraction process can affect the convergence of SM optimization. The uniqueness of this procedure can be improved by utilizing a good starting point. In the first iteration of the algorithm there is no available information about the mapping between the two spaces. A reasonable assumption is to take $\boldsymbol{x}_{os}^*$ as the starting point for the parameter extraction optimization problem. As the algorithm proceeds the matrix $\boldsymbol{B}^{(i)}$ approximates the mapping between the two spaces. A prediction of the extracted parameters in the *i*th iteration is given by

$$\boldsymbol{x}_{os}^{(p)} = \boldsymbol{x}_{os}^{(i)} + \boldsymbol{B}^{(i)} \left(\boldsymbol{x}_{em}^{(i+1)} - \boldsymbol{x}_{em}^{(i)} \right) \tag{25}$$

This predicted point is then taken as a starting point for the parameter extraction optimization problem. It supplies a good starting point provided that $\boldsymbol{x}_{os}^{(i)}$ is a valid solution to the parameter extraction in the previous iteration and $\boldsymbol{B}^{(i)}$ approximates the mapping between the two spaces.

VI. THE HASM ALGORITHM

The HASM algorithm exploits SM when effective, otherwise it defaults to direct optimization. Two objective functions are utilized by the algorithm. The first objective function is

$$\|\boldsymbol{f}\|_2^2 = \left\|\boldsymbol{P}(\boldsymbol{x}_{em}) - \boldsymbol{x}_{os}^*\right\|_2^2 \tag{26}$$

while the second function is

$$\|\boldsymbol{g}\|_2^2 = \left\|\boldsymbol{R}_{em}(\boldsymbol{x}_{em}) - \boldsymbol{R}_{os}(\boldsymbol{x}_{os}^*)\right\|_2^2 \tag{27}$$

While (26) aims at matching the extracted coarse model parameters to $\boldsymbol{x}_{os}^*$ in the parameter space, (27) aims at matching the same points mapped through the appropriate responses in the response space.

The HASM algorithm consists of two phases: the first phase follows the TRASM strategy while the second phase exploits direct optimization. It utilizes (18) and (19) for switching between phases as dictated by the smoothness of convergence.

In the *i*th iteration we assume the existence of a trusted extracted coarse model parameters $\boldsymbol{x}_{os}^{(i)} = \boldsymbol{P}(\boldsymbol{x}_{em}^{(i)})$. The step taken in this iteration is given by (7) where $\boldsymbol{x}_{em}^{(i+1)} = \boldsymbol{x}_{em}^{(i)} + \boldsymbol{h}^{(i)}$. Single-point parameter extraction is then applied at the point $\boldsymbol{x}_{em}^{(i+1)}$ to get $\boldsymbol{f}^{(i+1)} = \boldsymbol{P}(\boldsymbol{x}_{em}^{(i+1)}) - \boldsymbol{x}_{os}^*$.

The first phase utilizes two success criteria related to the reduction in (26) and (27). The SM success criterion is defined as

$$\left(\left\|\boldsymbol{f}^{(i)}\right\| - \left\|\boldsymbol{f}^{(i+1)}\right\|\right) > 0.01\left(\left\|\boldsymbol{f}^{(i)}\right\| - \left\|\boldsymbol{f}^{(i)} + \boldsymbol{B}^{(i)}\,\boldsymbol{h}^{(i)}\right\|\right) \tag{28}$$

which indicates that the actual reduction in the objective function (26) should be greater than a certain fraction of the predicted reduction. The direct optimization success criterion is

$$\left\|\boldsymbol{g}^{(i+1)}\right\| < \left\|\boldsymbol{g}^{(i)}\right\| \tag{29}$$

which implies that the new iterate $\boldsymbol{x}_{em}^{(i+1)}$ is a descent iterate of (27).

The new point $\boldsymbol{x}_{em}^{(i+1)}$ is accepted and the first phase resumes if this point satisfies both (28) and (29). $\boldsymbol{B}^{(i)}$ is then updated. The vector $\boldsymbol{f}^{(i+1)}$ satisfying (28) is either obtained through single-point extraction or through recursive multi-point extraction [3] that approaches a limit satisfying (28). We denote by $\boldsymbol{x}'_{em}$ and $\boldsymbol{R}'_{em}$ the solution obtained at the end of the first phase and the corresponding fine model response, respectively.

Switching to the second phase takes place in two cases. The first case is that (29) is not satisfied which means that we have to reject the new point $\boldsymbol{x}_{em}^{(i+1)}$. The Jacobian of the fine model response at the point $\boldsymbol{x}_{em}^{(i)}$ is then evaluated. This is done by first evaluating the Jacobian of the coarse model response $\boldsymbol{J}_{os}^{(i)}$ at the previously extracted coarse model point $\boldsymbol{x}_{os}^{(i)} = \boldsymbol{P}(\boldsymbol{x}_{em}^{(i)})$. $\boldsymbol{J}_{em}^{(i)}$ is then approximated using (18). The second phase is then supplied by $\boldsymbol{x}_{em}^{(i)}$, $\boldsymbol{J}_{em}^{(i)}$ and $\boldsymbol{f}^{(i)}$.

The second case occurs when the new point $\boldsymbol{x}_{em}^{(i+1)}$ satisfies (29) but does not satisfy (28). In this case the point $\boldsymbol{x}_{em}^{(i+1)}$ is better than the previous point $\boldsymbol{x}_{em}^{(i)}$ and is accepted. As the vector of extracted parameters does not satisfy (28), the vector $\boldsymbol{f}^{(i+1)}$ can not be trusted. In order to trust this vector, recursive multi-point parameter extraction is applied at the point $\boldsymbol{x}_{em}^{(i+1)}$ until either $\boldsymbol{f}^{(i+1)}$ approaches a limiting value or the number of additional points used for multi-point parameter extraction reaches *n*. If $\boldsymbol{f}^{(i+1)}$ approaches a limit that does not satisfy (28), $\boldsymbol{B}^{(i+1)}$ is updated, $\boldsymbol{J}_{os}^{(i+1)}$ at the extracted coarse model point $\boldsymbol{x}_{os}^{(i+1)} = \boldsymbol{P}(\boldsymbol{x}_{em}^{(i+1)})$ is evaluated and $\boldsymbol{J}_{em}^{(i+1)}$ is then approximated using (18). Otherwise, $\boldsymbol{J}_{em}^{(i+1)}$ is approximated using the *n*+1 fine model points used for multi-point parameter extraction. The second phase is then supplied by the point $\boldsymbol{x}_{em}^{(i+1)}$, $\boldsymbol{f}^{(i+1)}$ and the Jacobian estimate $\boldsymbol{J}_{em}^{(i+1)}$, which is either calculated using (18) or through finite differences.

The second phase utilizes the first-order derivatives supplied by SM to carry out a number of successful iterations. By a successful iteration we mean an iteration that satisfies the success criterion

$$\left(\left\|\boldsymbol{g}^{(k)}\right\| - \left\|\boldsymbol{g}^{(k+1)}\right\|\right) > 0.01\left(\left\|\boldsymbol{g}^{(k)}\right\| - \left\|\boldsymbol{g}^{(k)} + \boldsymbol{J}_{em}^{(k)}\boldsymbol{h}^{(k)}\right\|\right) \tag{30}$$

which indicates that the actual reduction in the objective function (27) should be greater than a certain fraction of the predicted reduction. Notice that the superscript k is used as an index for the successful iterates of the direct optimization phase. At the end of each successful iteration parameter extraction is applied at the new iterate $\boldsymbol{x}_{em}^{(k)}$ and is used to check whether a switch back to the first phase can take place. The criterion for such a switch is

$$\left\|\boldsymbol{f}^{(k+1)}\right\| < \left\|\boldsymbol{f}^{(k)}\right\| \tag{31}$$

If it is satisfied $\boldsymbol{J}_{os}^{(k+1)}$ is evaluated at the point $\boldsymbol{x}_{os}^{(k+1)} = \boldsymbol{P}(\boldsymbol{x}_{em}^{(k+1)})$, $\boldsymbol{B}$ is reevaluated using (19) and the algorithm switches back to the first phase. Otherwise, the second phase continues. We denote by $\boldsymbol{x}''_{em}$ and $\boldsymbol{R}''_{em}$ the solution obtained at the end of the second phase and the corresponding fine model response, respectively.

For any iteration $i \geq 0$, the two phases are given by the following steps.

Phase 1

Step 0 Given $\boldsymbol{x}_{em}^{(i)}$, $\boldsymbol{f}^{(i)}$, $\boldsymbol{B}^{(i)}$ and $d^{(i)}$. Set $d^{(i+1)} = d^{(i)}$.

Comment $d^{(i)}$ is the utilized trust region size.

Step 1 Obtain $\boldsymbol{h}^{(i)}$ by solving (7) with $d = d^{(i+1)}$. Let $d^{(i+1)} = \left\|\boldsymbol{h}^{(i)}\right\|_2$.

Step 2 Evaluate $\boldsymbol{x}_{em}^{(i+1)}$ using (5) and set $V = \{\boldsymbol{x}_{em}^{(i+1)}\}$.

Comment V is the set of fine model points utilized in the multi-point extraction.

Step 3 Apply multi-point parameter extraction using the points in the set V to obtain $\boldsymbol{f}^{(i+1)}$.

Comment The prediction given in (25) is used as a starting point for the multi-point parameter extraction.

Step 4 If both (28) and (29) are satisfied update the matrix $\boldsymbol{B}^{(i)}$ to $\boldsymbol{B}^{(i+1)}$ using Broyden's formula [6] and update d Go to Step 10.

Comment The trust region size $d$is updated based on how the predicted reduction in $\|\boldsymbol{f}\|_2$ agrees with the actual reduction [3].

Step 5 If (29) is not satisfied, obtain $\boldsymbol{J}_{os}^{(i)}$ and evaluate $\boldsymbol{J}_{em}^{(i)} = \boldsymbol{J}_{os}^{(i)} \boldsymbol{B}^{(i)}$. Switch to the second phase.

Comment The second phase takes as arguments $\boldsymbol{x}_{em}^{(i)}$, $\boldsymbol{f}^{(i)}$ and $\boldsymbol{J}_{em}^{(i)}$ and returns $\boldsymbol{x}_{em}^{(k)}$, $\boldsymbol{B}^{(k)}$ and $\boldsymbol{f}^{(k)}$. It should be clear that several iterations might be executed in the second phase before switching back to the first phase at Step 10.

Step 6 If $|V|$ is equal to one, go to Step 9.

Comment $|V|$ denotes the cardinality of the set *V*.

Step 7 Compare $\boldsymbol{f}^{(i+1)}$ obtained using $|V|$ fine model points with that previously obtained using $|V|-1$ fine model points. If $\boldsymbol{f}^{(i+1)}$ is approaching a limit, update the matrix $\boldsymbol{B}^{(i)}$ to get $\boldsymbol{B}^{(i+1)}$, obtain $\boldsymbol{J}_{os}^{(i+1)}$, evaluate $\boldsymbol{J}_{em}^{(i+1)} = \boldsymbol{J}_{os}^{(i+1)} \boldsymbol{B}^{(i+1)}$ and switch to the second phase.

Step 8 If $|V|$ is equal to *n*+1, obtain the matrix $\boldsymbol{J}_{em}^{(i+1)}$ by finite differences using the set *V*. Switch to the second phase.

Step 9 Obtain a temporary point $\boldsymbol{x}_t = \boldsymbol{x}_{em}^{(i+1)} + \boldsymbol{h}_t$, where

$$(\boldsymbol{B}^{(i)T} \boldsymbol{B}^{(i)} + l\, \boldsymbol{I})\, \boldsymbol{h}_t = -\boldsymbol{B}^{(i)T} \boldsymbol{f}^{(i+1)}$$

and $\|\boldsymbol{h}_t\| \le d^{(i+1)}$. Add this point to the set *V* and go to Step 3.

Step 10 Let *i*=*i*+1. Go to Step 0.

The second phase can be summarized in the following steps.

Phase 2

Step 0 Given the current iterate of the space mapping technique $\boldsymbol{x}_{em}^{(k)}$, the corresponding Jacobian matrix $\boldsymbol{J}_{em}^{(k)}$ and $\boldsymbol{f}^{(k)}$.

Step 1 Obtain a successful iterate $\boldsymbol{x}_{em}^{(k+1)}$ by solving

$$(\boldsymbol{J}_{em}^{(k)T}\boldsymbol{J}_{em}^{(k)}+\lambda\boldsymbol{I})\Delta\boldsymbol{x}=-\boldsymbol{J}_{em}^{(k)T}\boldsymbol{g}^{(k)}$$

for a suitable value of l that satisfies the direct optimization success criterion.

Step 2 Update $\boldsymbol{J}_{em}^{(k)}$ to $\boldsymbol{J}_{em}^{(k+1)}$.

Step 3 Apply parameter extraction at $\boldsymbol{x}_{em}^{(k+1)}$ to get $\boldsymbol{f}^{(k+1)}$.

Step 4 If (31) is satisfied obtain $\boldsymbol{J}_{os}^{(k+1)}$ at the point $\boldsymbol{x}_{os}^{(k+1)}=\boldsymbol{P}(\boldsymbol{x}_{em}^{(k+1)})$, evaluate the matrix $\boldsymbol{B}=\left(\boldsymbol{J}_{os}^{(k+1)T}\boldsymbol{J}_{os}^{(k+1)}\right)^{-1}\boldsymbol{J}_{os}^{(k+1)T}\boldsymbol{J}_{em}^{(k+1)}$ and switch to the first phase.

Step 5 If the termination condition is satisfied invoke the minimax optimizer else set $k=k+1$ and go to Step 1.

A flow chart of the first phase of the HASM algorithm is shown in Fig. 4.

To ensure optimality, direct optimization is used to solve the original design problem using a minimax optimizer [8] starting from $\boldsymbol{x}''_{em}$. The current implementation of the HASM algorithm is in MATLAB [9].

VII. EXAMPLES

Three-Section Waveguide Transformer

We consider the design of a three-section waveguide transformer [10]. The design constraints are

$$VSWR \le 1.04 \text{ for } 5.7 \text{ GHz} \le f \le 7.2 \text{ GHz} \tag{32}$$

The designable parameters are the heights of the waveguide sections b_1, b_2 and b_3 and the lengths of waveguide sections L_1, L_2 and L_3. The fine model exploits HP HFSS [11] through HP Empipe3D [12]. The coarse analytical model does not take into account the junction discontinuity effects [10].

The vector $\boldsymbol{x}_{os}^{*}$ is taken as the initial fine model design (Fig. 5). The HASM algorithm switched to the second phase after two iterations of the first phase, which required 4 fine model simulations. The

response $\boldsymbol{R}'_{em}$ is shown in Fig. 6. The second phase carried out only one iteration which required 2 fine model simulations. The response $\boldsymbol{R}''_{em}$ is shown in Fig. 7.

Direct minimax optimization is then applied to the original design problem. The optimal fine model response $\boldsymbol{R}^*_{em}$ is shown in Fig. 8. Figs. 6 and 8 show that in this example $\boldsymbol{R}'_{em}$ is different from $\boldsymbol{R}^*_{em}$. The designs $\boldsymbol{x}^*_{os}$, $\boldsymbol{x}'_{em}$, $\boldsymbol{x}''_{em}$ and $\boldsymbol{x}^*_{em}$ are shown in Table I.

Six-Section H-Plane Waveguide Filter

We consider a six-section H-plane waveguide filter [13, 14]. Design specifications are taken as

$$|S_{11}| \le 0.16 \quad \text{for} \quad 5.4 \text{ GHz} \le f \le 9.0 \text{ GHz} \tag{33}$$

$$|S_{11}| \ge 0.85 \quad \text{for } f \le 5.2 \text{ GHz} \quad \text{and } |S_{11}| \ge 0.5 \quad \text{for } 9.5 \text{ GHz} \le f \tag{34}$$

A waveguide with a cross-section of 1.372 inches by 0.622 inches (3.485 cm by 1.58 cm) is used. The six sections are separated by seven H-plane septa, which have a finite thickness of 0.02 inches (0.508 mm). The filter is shown in Fig. 9.

The optimizable parameters are the four septa widths W_1, W_2, W_3 and W_4 and the three waveguide-section lengths L_1, L_2 and L_3. The coarse model consists of lumped inductances and dispersive transmission line sections. It is simulated using OSA90/hope [15]. There are various approaches to calculate the equivalent inductive susceptance corresponding to an H-plane septum. We utilize a simplified version of a formula due to Marcuvitz [16] in evaluating the inductances. The coarse model is shown in Fig. 10. The fine model exploits HP HFSS [11] through HP Empipe3D [12].

The fine model response at the starting point $\boldsymbol{x}^*_{os}$ is shown in Fig. 11. The first phase required 4 iterations to reach the design $\boldsymbol{x}'_{em}$. A total of 5 fine model simulations were needed. The second phase did not carry out any successful iteration. The response $\boldsymbol{R}''_{em}$ is shown in Fig. 12.

The response $\boldsymbol{R}_{em}^{*}$ is obtained through direct minimax optimization (see Fig. 13). The different fine model designs are given in Table II. It is clear that the convergence of the first phase is smooth as $\boldsymbol{R}'_{em} \approx \boldsymbol{R}_{em}^{*} \approx \boldsymbol{R}_{os}^{*}$.

Seven-Section Waveguide Transformer

The design of a seven-section waveguide transformer is also considered. The transformer is shown in Fig. 14. This example is a classical microwave circuit design problem [10]. The fine model is simulated using HP HFSS [11] through HP Empipe3D [12]. The coarse model is an analytical model which neglects the junction discontinuity [10]. The design specifications are taken as

$$VSWR \le 1.01 \quad \text{for} \quad 1.06 \text{ GHz} \le f \le 1.8 \text{ GHz} \tag{35}$$

The designable parameters for this problem are the height and length of each waveguide section. The fine model response at $\boldsymbol{x}_{os}^{*}$ is shown in Fig. 15. The first phase executed three successful iterations that required six fine model simulations. The response $\boldsymbol{R}'_{em}$ is shown in Fig. 16. The second phase executed four iterations (see Fig. 17). The response $\boldsymbol{R}_{em}^{*}$ is shown in Fig. 18. Table III shows the different designs.

Double-Folded Stub Filter

We consider the design of the double-folded stub (DFS) microstrip structure (Bandler *et al*. [1]). Folding the stubs reduces the filter area w.r.t. the conventional double stub structure (Rautio [17]). The filter is characterized by five parameters : W_1, W_2, S, L_1 and L_2 (see Fig. 19). L_1, L_2 and S are chosen as optimization variables. W_1 and W_2 are fixed at 4.8 mil. The design specifications are

$$|S_{21}| \ge -3 \text{ dB} \quad \text{for} \quad f \le 9.5 \text{ GHz} \quad \text{and} \quad 16.5 \text{ GHz} \le f \tag{36}$$

$$|S_{21}| \le -30 \text{ dB} \quad \text{for} \quad 12 \text{ GHz} \le f \le 14 \text{ GHz} \tag{37}$$

The fine model is the structure simulated by HP HFSS [11] through HP Empipe3D [12]. The coarse model exploits the microstrip line and microstrip T-junction models available in OSA90/hope [15]. The coupling between the folded stubs and the microstrip line is simulated using equivalent

capacitors. The values of these capacitors are determined using Walker's formulas [18]. Jansen's microstrip bend model [19] is used to model the folding effect of the stub. The coarse model is shown in Fig. 20.

The fine model response at $\boldsymbol{x}_{os}^{*}$ is shown in Fig. 21. This figure shows a big shift between the optimal coarse response and the initial fine response. This signals considerable misalignment between the two models.

The first phase successfully carried out eight iterations that required twelve fine model simulations. The response $\boldsymbol{R}_{em}'$ is shown in Fig. 22. Fig. 23 shows a coarse contour plot of $\|\boldsymbol{f}\|_2^2$ in the neighborhood of the point of $\boldsymbol{x}_{em}'$. It is clear from this figure that the first phase was trapped in a local minimum. The mapping established in the first phase is utilized to get a good estimate of $\boldsymbol{J}_{em}$ and a switch to the second phase is carried out. The response $\boldsymbol{R}_{em}''$ (Fig. 24) shows a significant improvement in the response. The design $\boldsymbol{x}_{em}''$ is then taken as the starting point for the minimax optimizer. The response $\boldsymbol{R}_{em}^{*}$ is shown in Fig. 25. The designs are given in Table IV.

VIII. CONCLUSIONS

We present a novel Hybrid Aggressive Space Mapping (HASM) optimization algorithm. The algorithm is designed to handle severely misaligned cases. It enables smooth switching from SM optimization to direct optimization if SM fails. The direct optimization phase utilizes all the available information accumulated by SM optimization about the mapping between the coarse and fine model spaces. The algorithm also enables switching back from direct optimization to space mapping if SM is converging smoothly. The connection between SM and direct optimization is based on a novel lemma. An original approach for the prediction of the starting point of the parameter extraction optimization problem is also utilized. This approach improves the uniqueness of the extraction step and consequently

enhances the convergence of the algorithm. The algorithm is successfully demonstrated through the design of waveguide transformers and filters.

ACKNOWLEDGEMENT

The authors thank HP EEsof, Santa Rosa, CA, for making HP HFSS and HP Empipe3D available for this work.

REFERENCES

[1] J.W. Bandler, R.M. Biernacki, S.H. Chen, P.A. Grobelny and R.H. Hemmers, "Space mapping technique for electromagnetic optimization," *IEEE Trans. Microwave Theory Tech.*, vol. 42, 1994, pp. 2536-2544.

[2] J.W. Bandler, R.M. Biernacki and S.H. Chen, "Fully automated space mapping optimization of 3D structures," *IEEE MTT-S Int. Microwave Symp. Dig.* (San Francisco, CA), 1996, pp. 753-756.

[3] M.H. Bakr, J.W. Bandler, R.M. Biernacki, S.H. Chen and K. Madsen, "A trust region aggressive space mapping algorithm for EM optimization," *IEEE Trans. Microwave Theory Tech.*, vol. 46, 1998, pp. 2412-2425.

[4] J.W. Bandler, R.M. Biernacki, S.H. Chen, R.H. Hemmers and K. Madsen, "Electromagnetic optimization exploiting aggressive space mapping," *IEEE Trans. Microwave Theory Tech.*, vol. 43, 1995, pp. 2874-2882.

[5] J.J. Moré and D.C. Sorenson, "Computing a trust region step," *SIAM J. Sci. Stat. Comp.*, vol. 4, 1983, pp. 553-572.

[6] C.G. Broyden, "A class of methods for solving nonlinear simultaneous equations," *Math. Comp.*, vol. 19, 1965, pp. 577-593.

[7] R. Fletcher, *Practical Methods of Optimization*, New York: Wiley, Second Edition, 1987.

[8] J.W. Bandler, W. Kellermann and K. Madsen, "A superlinearly convergent minimax algorithm for microwave circuit design," *IEEE Trans. Microwave Theory Tech.*, vol. MTT-33, 1985, pp. 1519-1530.

[9] MATLAB® Version 5.0, The Math. Works, Inc., 24 Prime Park Way, Natick, MA 01760, 1997.

[10] J.W. Bandler, "Computer optimization of inhomogeneous waveguide transformers," *IEEE Trans. Microwave Theory Tech.*, vol. MTT-17, 1969, pp. 563-571.

[11] HP HFSS™ Version 5.2, HP EEsof Division, 1400 Fountaingrove Parkway, Santa Rosa, CA 95403-1799, 1998.

[12] HP Empipe3D™ Version 5.2, HP EEsof Division, 1400 Fountaingrove Parkway, Santa Rosa, CA 95403-1799, 1998.

[13] L. Young and B.M. Schiffman, "A useful high-pass filter design," *Microwave J.*, vol. 6, 1963, pp. 78-80.

[14] G.L. Matthaei, L. Young and E.M. T. Jones, *Microwave Filters, Impedance-Matching Network and Coupling Structures*. New York: McGraw-Hill, First Edition, 1964.

[15] OSA90/hope™ Version 4.0, formerly Optimization Systems Associates Inc., P.O. Box 8083, Dundas, ON, Canada, L9H 5E7, 1997, now HP EEsof Division, 1400 Fountaingrove Parkway, Santa Rosa, CA 95403-1799.

[16] N. Marcuvitz, *Waveguide Handbook*. New York: McGraw-Hill, First Edition, 1951, p. 221.

[17] J.C. Rautio, Sonnet Software, Inc., 1020 Seventh North Street, Suite 210, Liverpool, NY 13088, Private Communication, 1992.

[18] C.S. Walker, Capacitance, Inductance and Crosstalk Analysis, Norwood, MA: Artech House, 1990.

[19] M. Kirschning, R. Jansen and N. Koster, "Measurement and computer-aided modeling of microstrip discontinuities by an improved resonator method," *IEEE MTT-S Int. Microwave Symp. Dig*. (Boston, MA), 1983, pp. 495-497.

TABLE I
THE OPTIMAL COARSE MODEL DESIGN AND THE DESIGNS OBTAINED DURING DIFFERENT PHASES OF THE HASM ALGORITHM FOR THE THREE-SECTION WAVEGUIDE TRANSFORMER

Parameter	$\boldsymbol{x}_{os}^{*}$	$\boldsymbol{x}'_{em}$	$\boldsymbol{x}''_{em}$	$\boldsymbol{x}_{em}^{*}$
b_1	0.90318	0.90331	0.90114	0.90549
b_2	1.37093	1.36436	1.35687	1.35777
b_3	1.73609	1.73208	1.72470	1.71866
L_1	1.54879	1.46991	1.47203	1.47008
L_2	1.58375	1.56402	1.56521	1.57587
L_3	1.64590	1.79666	1.77744	1.78286

All values are in cm

TABLE II
THE OPTIMAL COARSE MODEL DESIGN, THE FINAL SPACE-MAPPED AND THE OPTIMAL FINE MODEL DESIGNS FOR THE SIX-SECTION H-PLANE WAVEGUIDE FILTER

Parameter	$\boldsymbol{x}_{os}^{*}$	$\boldsymbol{x}'_{em}$, $\boldsymbol{x}''_{em}$	$\boldsymbol{x}_{em}^{*}$
W_1	0.48583	0.51326	0.51344
W_2	0.43494	0.47379	0.47396
W_3	0.40433	0.45091	0.45100
W_4	0.39796	0.44675	0.44664
L_1	0.65585	0.63701	0.63695
L_2	0.65923	0.63954	0.63977
L_3	0.67666	0.65704	0.65694

All values are in inches

TABLE III
THE OPTIMAL COARSE MODEL DESIGN AND THE DESIGNS OBTAINED DURING DIFFERENT PHASES OF THE HASM ALGORITHM FOR THE SEVEN-SECTION WAVEGUIDE TRANSFORMER

Parameter	$\boldsymbol{x}_{os}^{*}$	$\boldsymbol{x}'_{em}$	$\boldsymbol{x}''_{em}$	$\boldsymbol{x}_{em}^{*}$
b_1	7.86732	7.84126	7.84321	7.84319
b_2	6.61888	6.56661	6.56753	6.56746
b_3	4.68540	4.63369	4.63275	4.63267
b_4	2.91987	2.88266	2.88266	2.88268
b_5	1.81412	1.79307	1.79273	1.79272
b_6	1.27658	1.26697	1.26721	1.26723
b_7	1.06847	1.06475	1.06477	1.06474
L_1	7.10588	7.27059	7.27141	7.27145
L_2	7.12201	7.03866	7.04043	7.04047
L_3	7.11760	6.89568	6.89549	6.89552
L_4	7.12331	6.89253	6.89192	6.89189
L_5	7.12815	6.98273	6.97985	6.98000
L_6	7.12154	7.03160	7.03020	7.03023
L_7	7.12945	7.02606	7.02503	7.02509

All values are in cm

TABLE IV
THE OPTIMAL COARSE MODEL DESIGN, THE FINAL SPACE-MAPPED AND THE OPTIMAL FINE MODEL DESIGNS FOR THE DFS FILTER

Parameter	$\boldsymbol{x}_{os}^{*}$	$\boldsymbol{x}'_{em}$	$\boldsymbol{x}''_{em}$	$\boldsymbol{x}_{em}^{*}$
L_1	66.727	72.454	73.869	78.964
L_2	60.228	72.728	82.939	81.210
S	9.592	7.621	8.170	7.901

All values are in mil

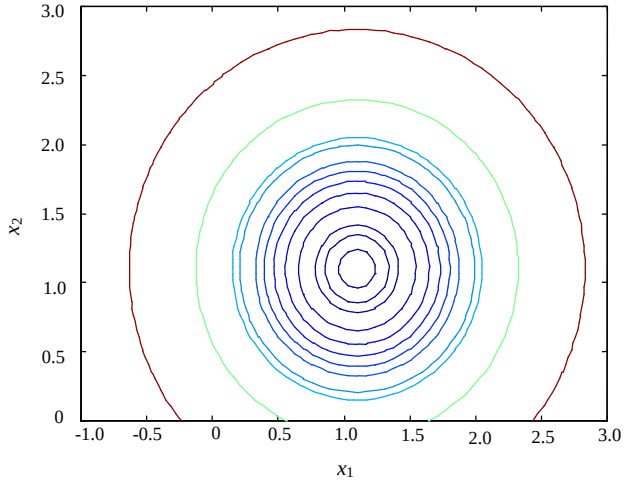

(a)

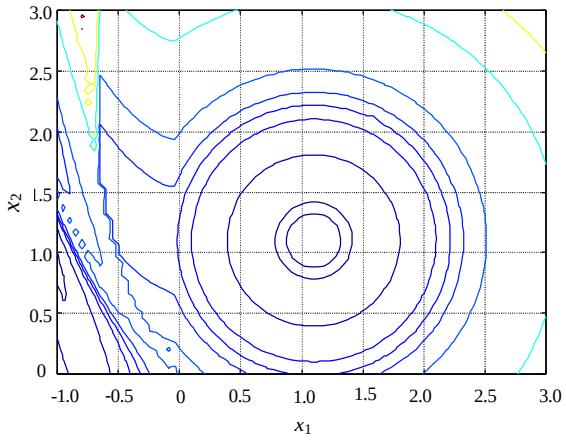

(b)

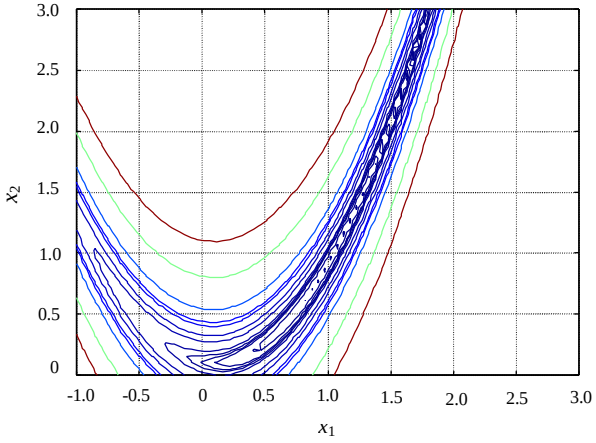

(c)

Fig. 1. Different contour plots for the Rosenbrock problem for the case a = [–0.1 –0.1]^T; (a) the contour plot of $\left\|\boldsymbol{x}_{em}+a-\boldsymbol{x}_{os}^{*}\right\|_2^2$, (b) the contour plot of $\left\|\boldsymbol{P}(\boldsymbol{x}_{em})-\boldsymbol{x}_{os}^{*}\right\|_2^2$ obtained through parameter extraction and (c) contours of the fine model Rosenbrock function.

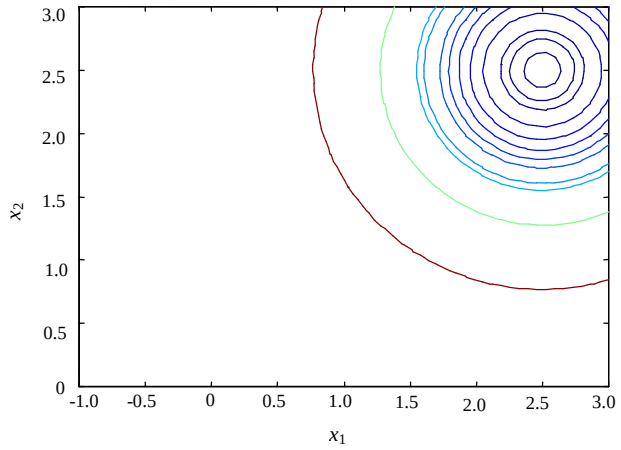

(a)

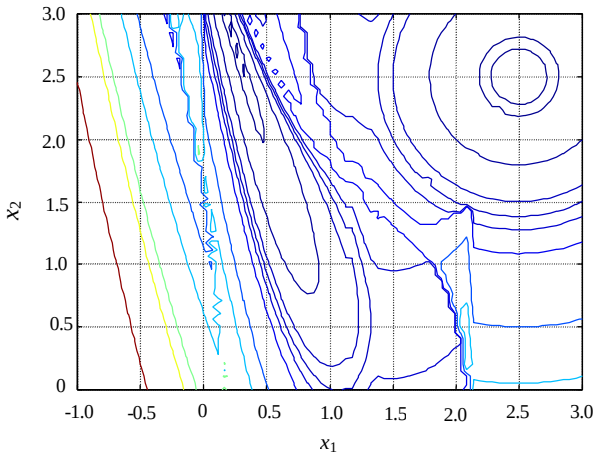

(b)

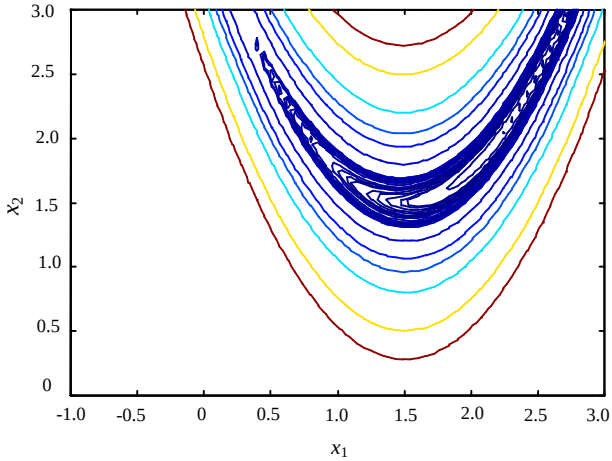

(c)

Fig. 2. Different contour plots for the Rosenbrock problem for the case $a = [-1.5 \quad -1.5]^T$; (a) the contour plot of $\left\|\boldsymbol{x}_{em}+a-\boldsymbol{x}_{os}^*\right\|_2^2$, (b) the contour plot of $\left\|\boldsymbol{P}(\boldsymbol{x}_{em})-\boldsymbol{x}_{os}^*\right\|_2^2$ obtained through parameter extraction and (c) contours of the fine model Rosenbrock function.

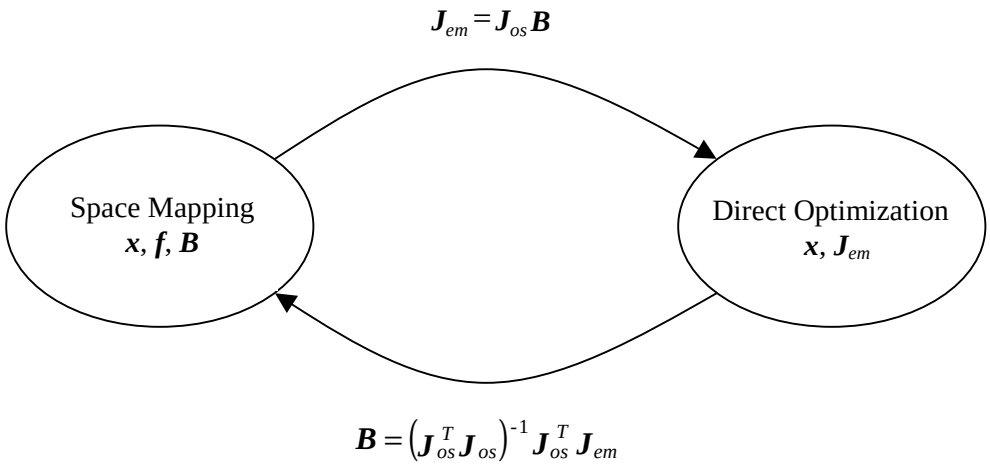

Fig. 3. Illustration of the connection between SM optimization and direct optimization.

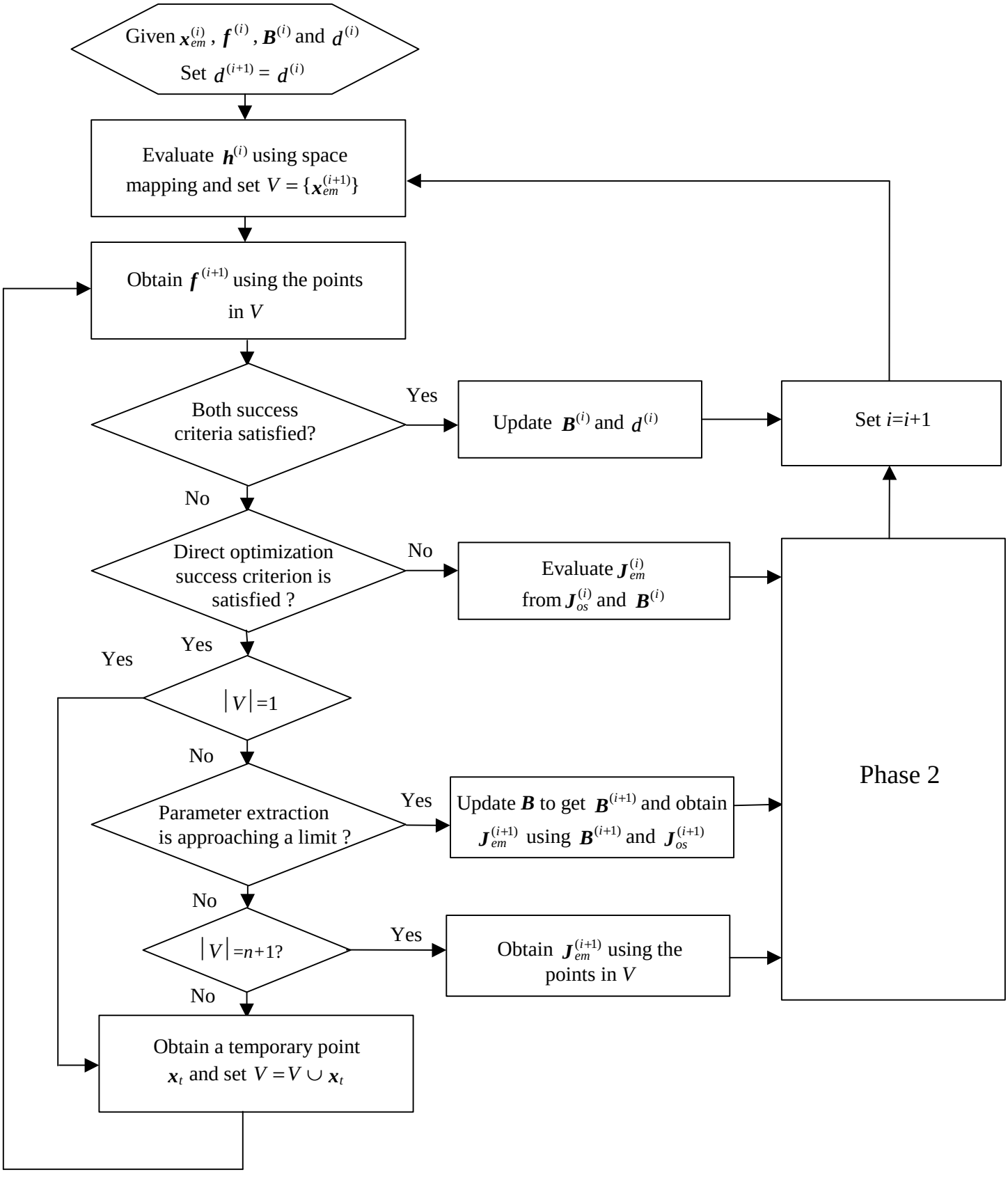

Fig. 4. A flow chart of the first phase of the proposed algorithm.

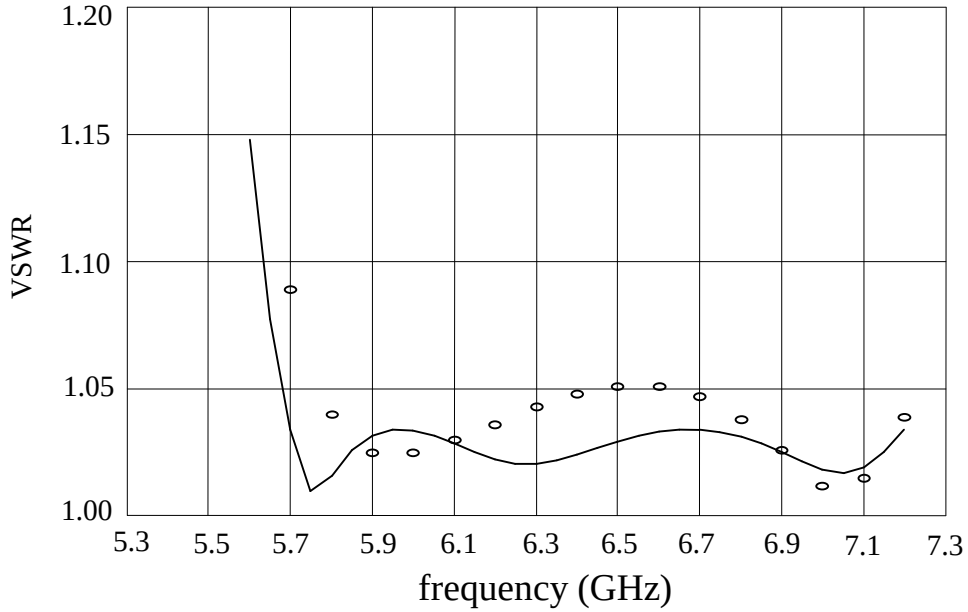

Fig. 5. The coarse response $\boldsymbol{R}_{os}^{*}$ (—) and the fine response $\boldsymbol{R}_{em}(\boldsymbol{x}_{os}^{*})$ (o) for the three-section waveguide transformer.

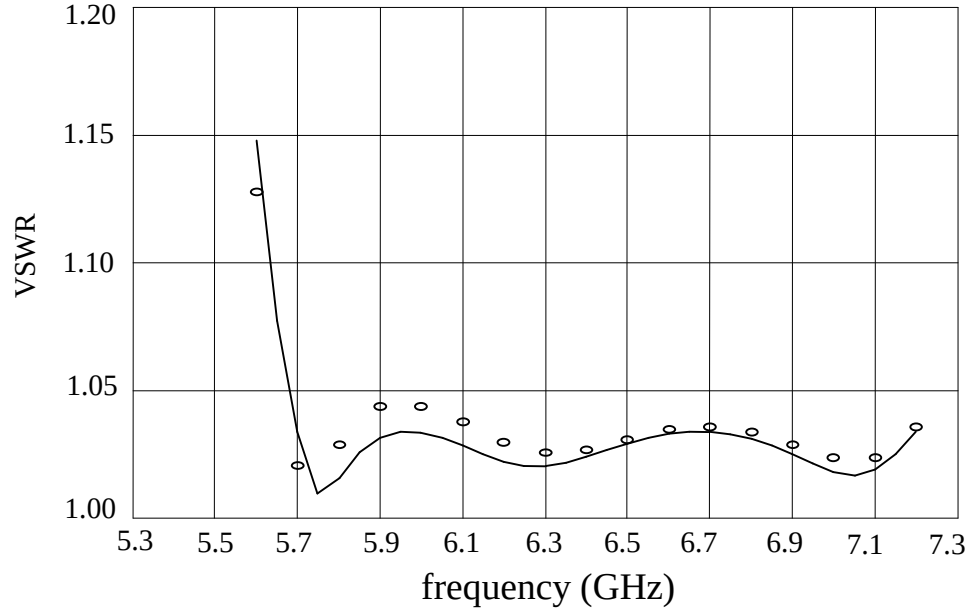

Fig. 6. The coarse response $\boldsymbol{R}_{os}^{*}$ (—) and the fine response $\boldsymbol{R}'_{em}$ (o) for the three-section waveguide transformer.

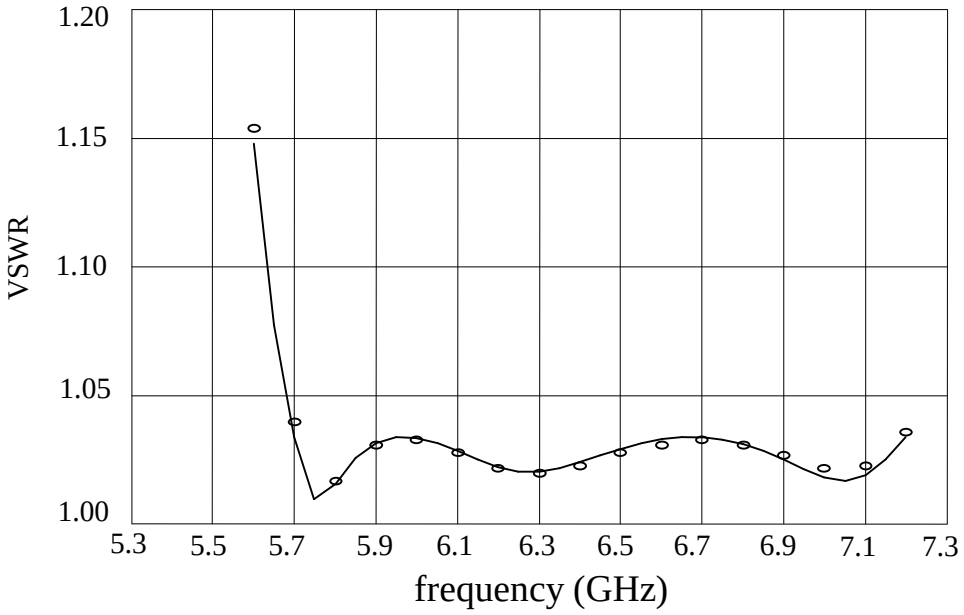

Fig. 7. The coarse response $\boldsymbol{R}_{os}^{*}$ (—) and the fine response $\boldsymbol{R}_{em}''$ (o) for the three-section waveguide transformer.

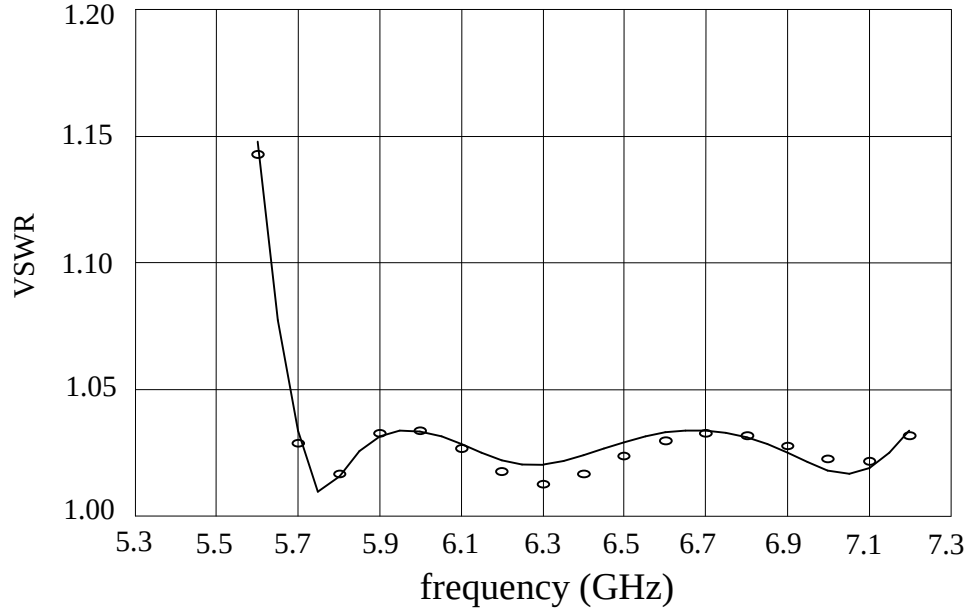

Fig. 8. The coarse response $\boldsymbol{R}_{os}^{*}$ (—) and the fine response $\boldsymbol{R}_{em}^{*}$ (o) for the three-section waveguide transformer.

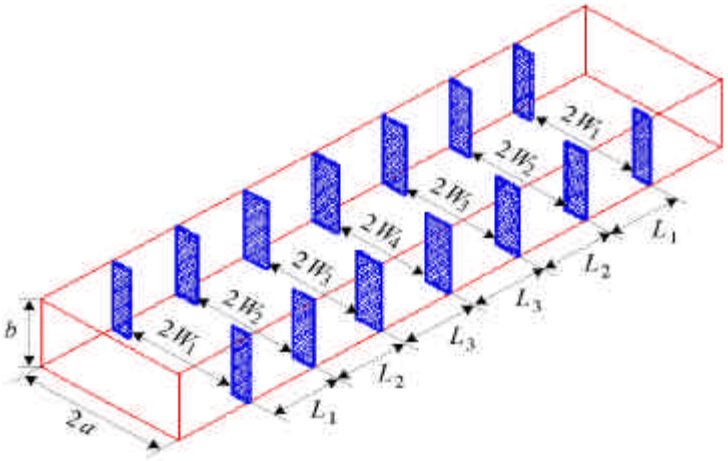

Fig. 9. The fine model of the six-section H-plane waveguide filter [13, 14].

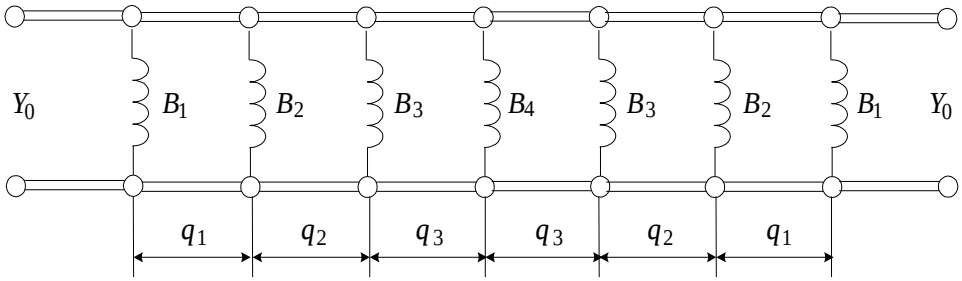

Fig. 10. The coarse model of the six-section H-plane waveguide filter [16].

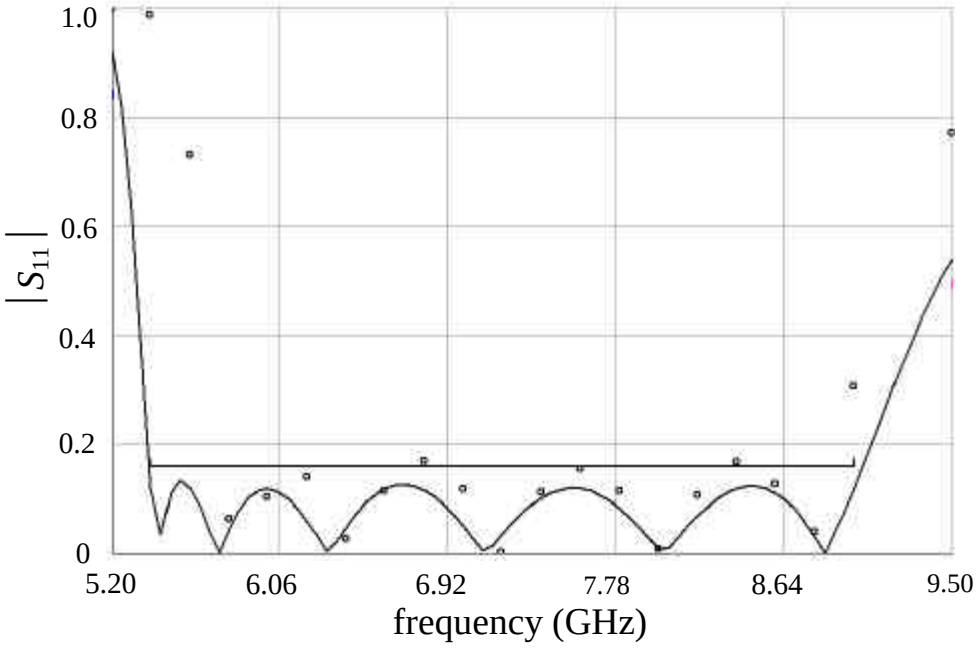

Fig. 11. The coarse response $\boldsymbol{R}_{os}^{*}$ (—) and the fine response $\boldsymbol{R}_{em}(\boldsymbol{x}_{os}^{*})$ (o) for the six-section H-plane waveguide filter.

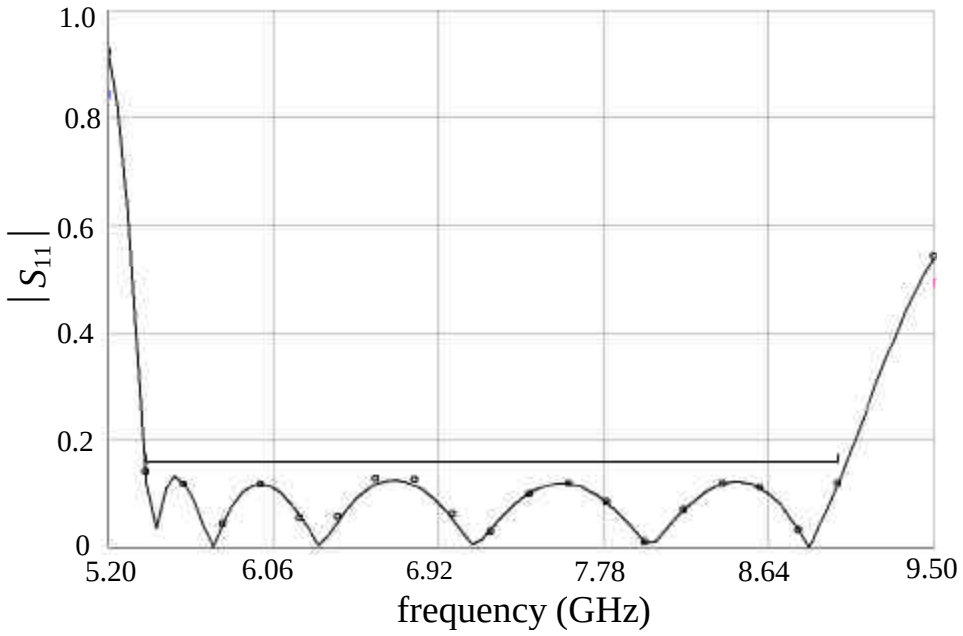

Fig. 12. The coarse response $\boldsymbol{R}_{os}^{*}$ (—) and the fine response $\boldsymbol{R}_{em}''$ (o) for the six-section H-plane waveguide filter.

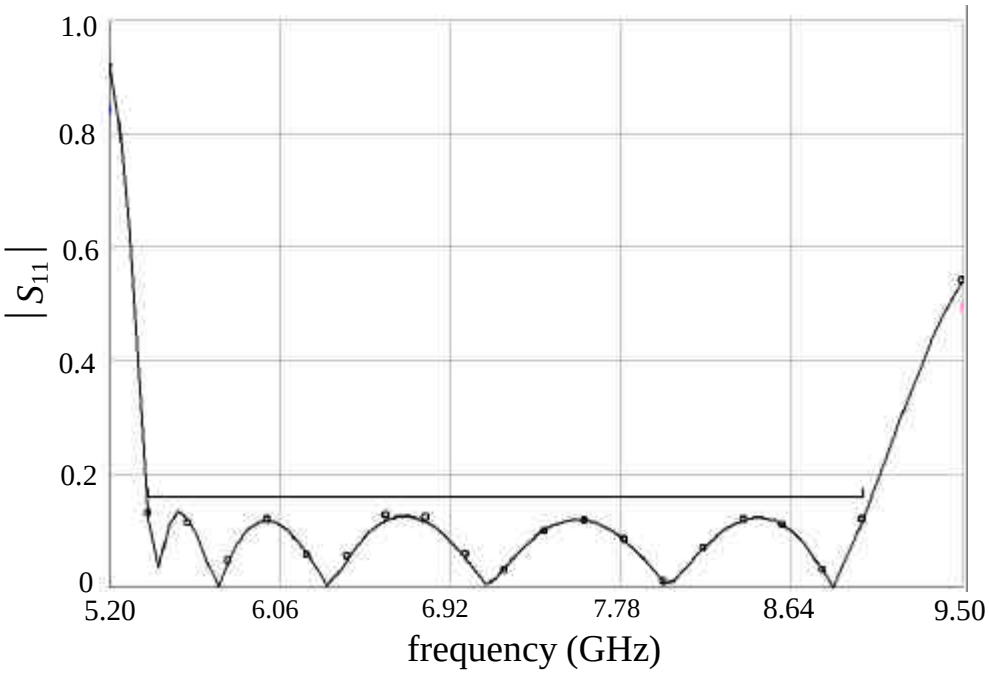

Fig. 13. The coarse response $\boldsymbol{R}_{os}^{*}$ (—) and the fine response $\boldsymbol{R}_{em}^{*}$ (o) for the six-section H-plane waveguide filter.

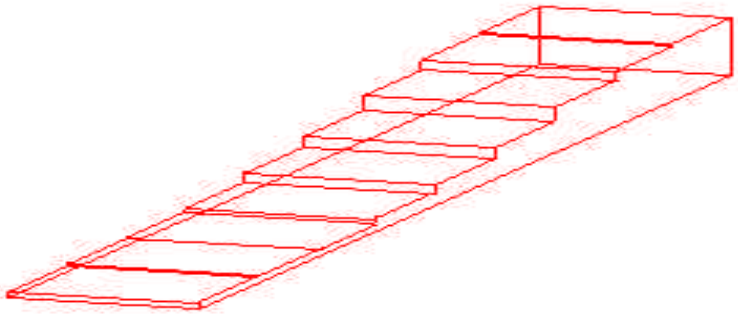

Fig. 14. The seven-section waveguide transformer [10].

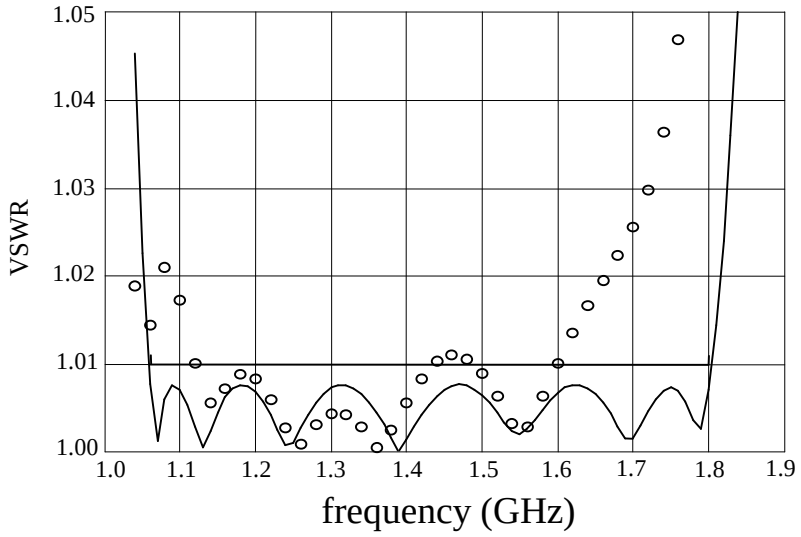

Fig. 15. The coarse response $\boldsymbol{R}_{os}^{*}$ (—) and the fine response $\boldsymbol{R}_{em}(\boldsymbol{x}_{os}^{*})$ (o) for the seven-section waveguide transformer.

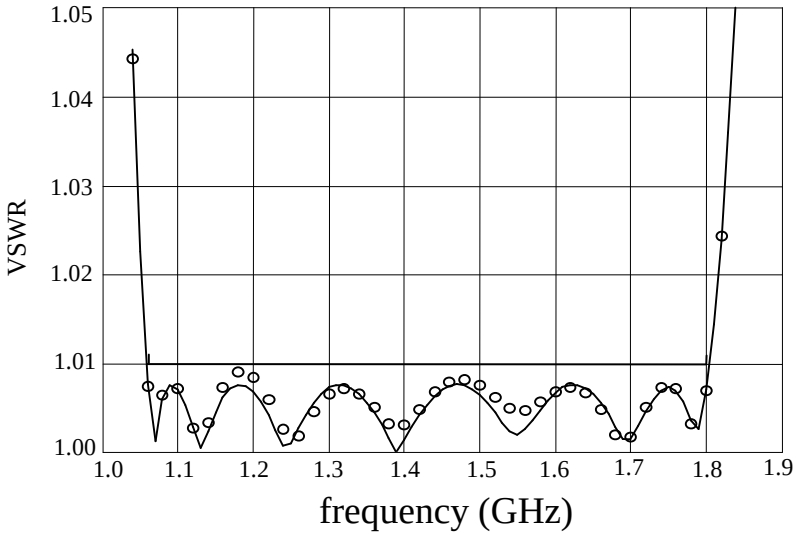

Fig. 16. The coarse response $\boldsymbol{R}_{os}^{*}$ (—) and the fine response $\boldsymbol{R}_{em}'$ (o) for the seven-section waveguide transformer.

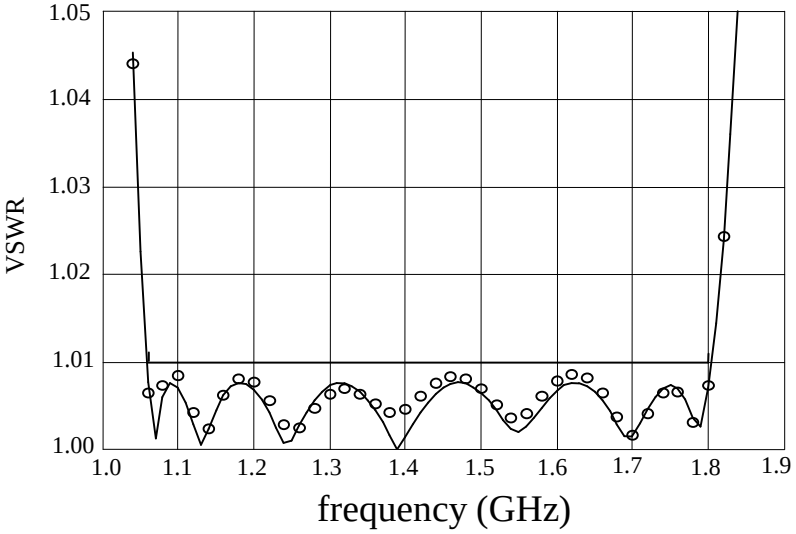

Fig. 17. The coarse response $\boldsymbol{R}_{os}^{*}$ (—) and the fine response $\boldsymbol{R}_{em}''$ (o) for the seven-section waveguide transformer.

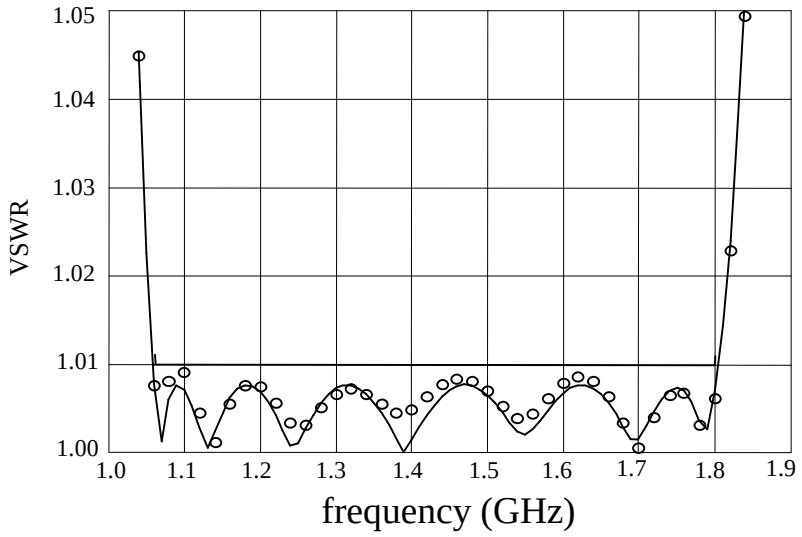

Fig. 18. The coarse response $\boldsymbol{R}_{os}^{*}$ (—) and the fine response $\boldsymbol{R}_{em}^{*}$ (o) for the seven-section waveguide transformer.

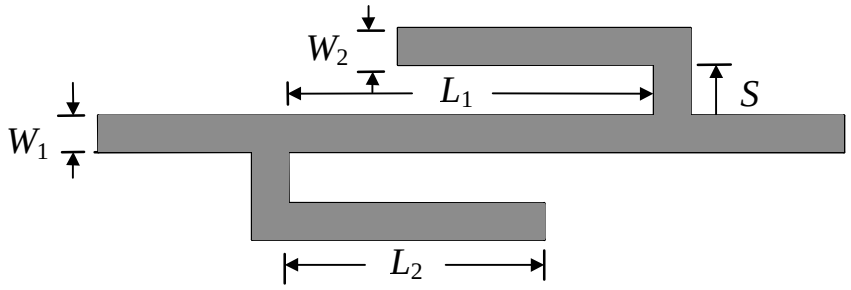

Fig. 19. The DFS filter [1, 17].

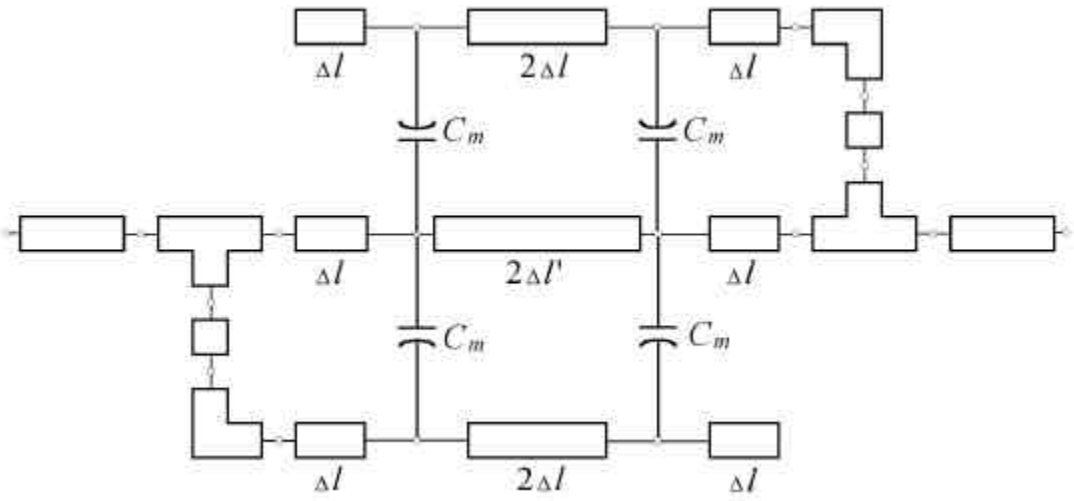

Fig. 20. The coarse model of the DFS filter.

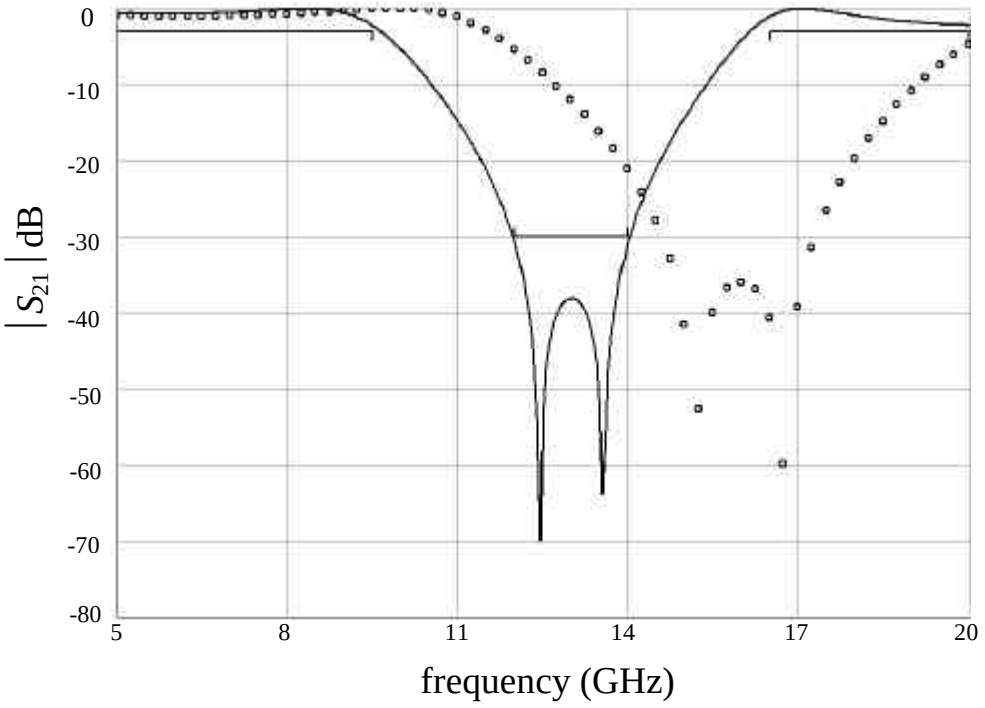

Fig. 21. The coarse response $\boldsymbol{R}_{os}^{*}$ (—) and the fine response $\boldsymbol{R}_{em}(\boldsymbol{x}_{os}^{*})$ (o) for the DFS filter.

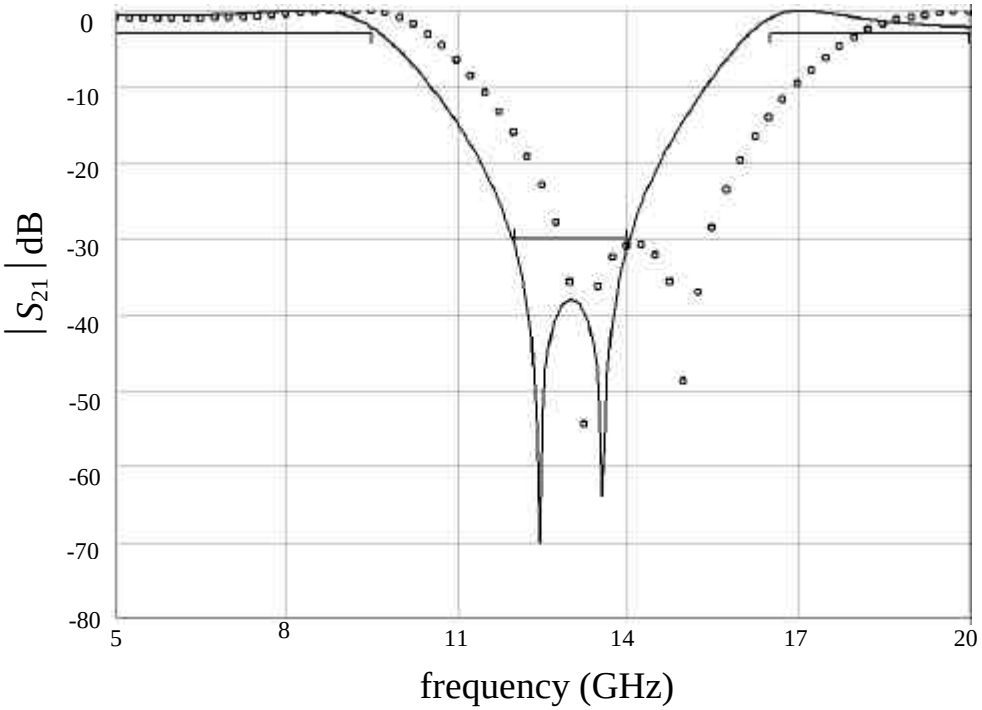

Fig. 22. The coarse response $\boldsymbol{R}_{os}^{*}$ (—) and the fine response $\boldsymbol{R}'_{em}$ (o) for the DFS filter.

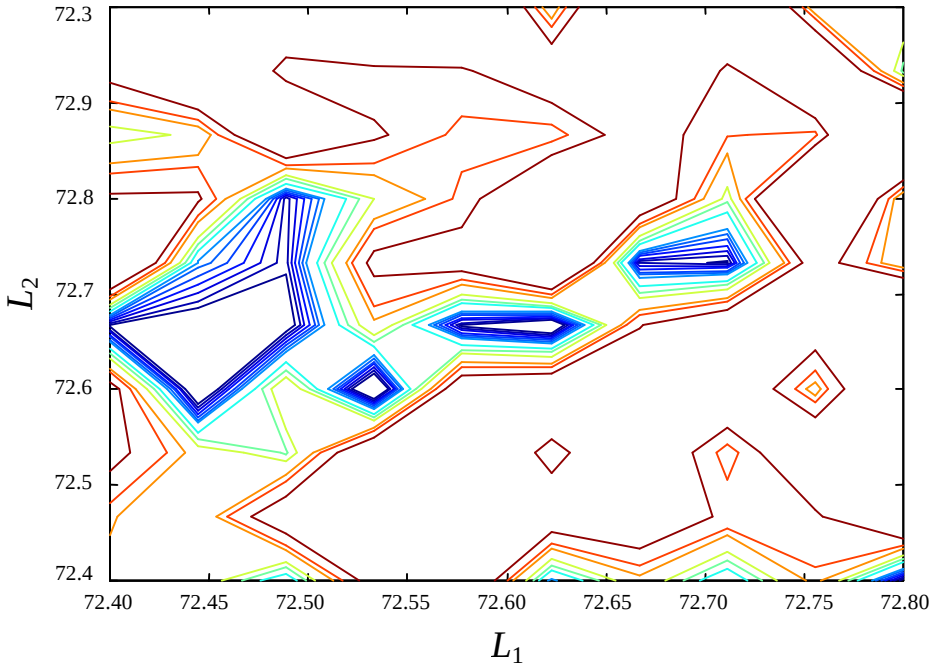

Fig. 23. A coarse contour plot of $\left\| \boldsymbol{P}(\boldsymbol{x}_{em}) - \boldsymbol{x}_{os}^{*} \right\|_2^2$ in the neighborhood of $\boldsymbol{x}'_{em}$ for the DFS filter.

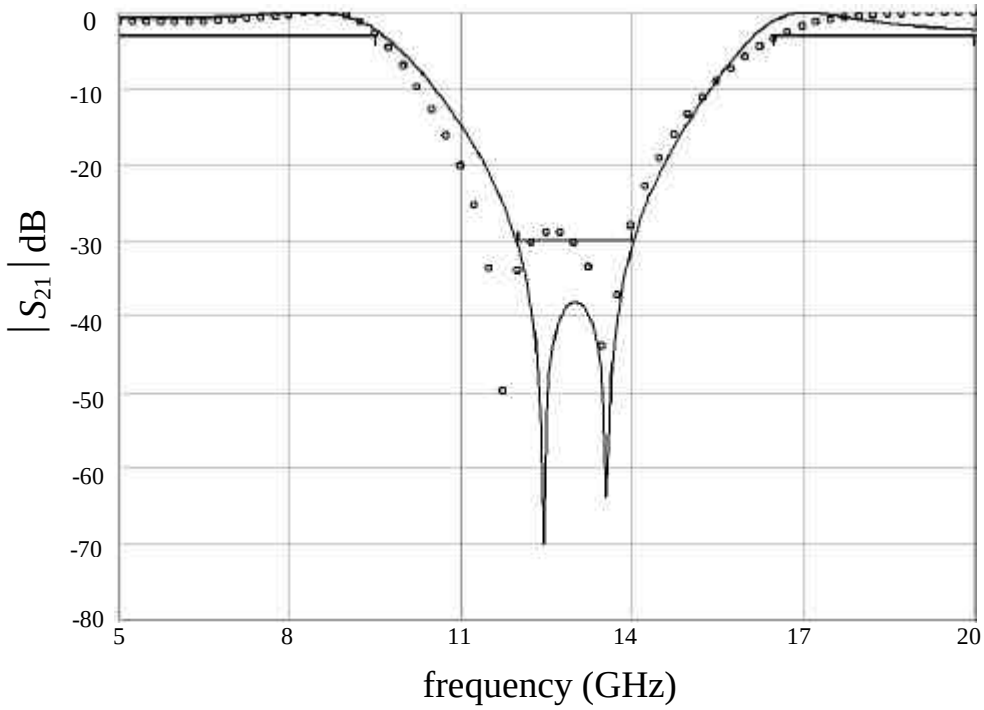

Fig. 24. The coarse response $\boldsymbol{R}_{os}^{*}$ (—) and the fine response $\boldsymbol{R}''_{em}$ (o) for the DFS filter.

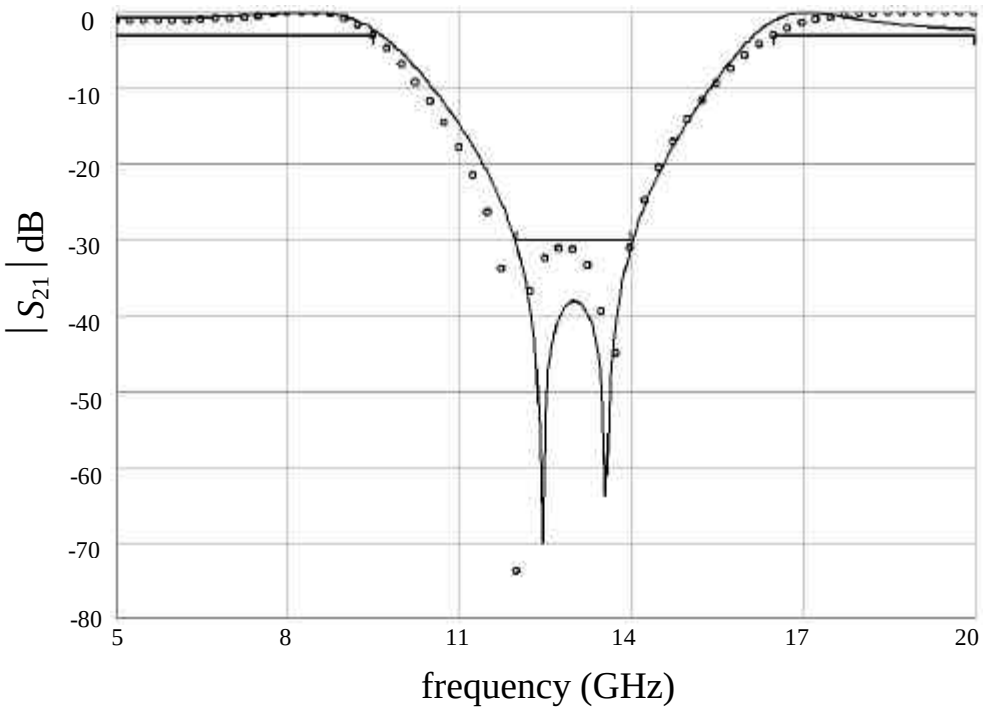

Fig. 25. The coarse response $\boldsymbol{R}_{os}^{*}$ (—) and the fine response $\boldsymbol{R}_{em}^{*}$ (o) for the DFS filter.